

Article

The Crucial Role of Quaternary Mixtures of Active Layer in Organic Indoor Solar Cells

Premkumar Vincent ¹, Jae Won Shim ², Jaewon Jang ¹, In Man Kang ¹, Philippe Lang ³, Jin-Hyuk Bae ^{1,*} and Hyeok Kim ^{4,*}

¹ School of Electronics Engineering, Kyungpook National University, 80 Daehakro, Bukgu, Daegu 41566, Korea; vinprekumar@gmail.com (P.V.); jljang@knu.ac.kr (J.J.); imkang@ee.knu.ac.kr (I.M.K.)

² Research Center for Photoenergy Harvesting & Conversion Technology (phct), Division of Electronics and Electrical Engineering, Dongguk University, Seoul 04620, Korea; jwshim@dongguk.edu

³ ITODYS University Paris Diderot CNRS UMR 7086 (Paris 7), 75013 Paris, France; lang@univ-paris-diderot.fr

⁴ Department of Electrical Engineering, Engineering Research Institute (ERI), Gyeongang National University, 501 Jinjudaero, Jinju, Gyeongnam 52828, Korea

* Correspondence: jhbae@ee.knu.ac.kr (J.-H.B.); hyeok.kim@gnu.ac.kr (H.K.)

Received: 18 March 2019; Accepted: 13 May 2019; Published: 15 May 2019



Abstract: A bulk heterojunction (BHJ) consisting of more than one donor/acceptor is one plausible way to improve the charge transport and/or the spectral absorption range in organic solar cells. Ternary and quaternary solar cells have shown promise in this regard. However, quaternary structures have not yet been intensively tested under indoor lighting conditions. A finite-difference time-domain (FDTD)-based simulation was used to solve for the electric field intensity distribution inside a quaternary photovoltaic device illuminated by 500 lx indoor white light emitting diodes (LEDs). We found that quaternary indoor photovoltaics (IPVs) showed peculiarly high oscillations in the simulated ideal short-circuit current density ($J_{sc,ideal}$). Here, we simulated the electric field intensity inside the photovoltaic, compared it to single BHJ photovoltaics, and deduced that the electric field intensity inside the active layer of the IPV was highly sensitive to its thickness due to interference between the incident light and the light reflecting from the back electrode. We also found that Poly[N-9'-hepta-decanyl-2,7-carbazole-alt-5,5-(4',7'-di-2-thienyl-2',1',3'-benzothiadiazole)] (PCDTBT) acted as the primary light absorber in the quaternary blend while poly([4,8-bis[(2-ethylhexyl)oxy]benzo[1,2-b:4,5-b']dithiophene-2,6-diyl){3-fluoro-2-[(2-ethylhexyl)carbonyl]thieno[3,4-b]thiophenediyl}) (PTB7) acted primarily as a cascade energy level and secondarily as a supplementary light absorber.

Keywords: quaternary; organic; finite-difference time-domain; optical modeling; layer thickness optimization

1. Introduction

Due to rapid development in the industry of wireless sensors and the internet of things (IoT), the number of portable devices connected to networks has substantially increased [1–3]. Although fast-charging, lightweight batteries are being developed, these batteries still do not completely overcome the limited operation time of such portable devices. In order to overcome this issue, micro-power harvesting technologies such as thermoelectric, piezoelectric, photovoltaic, and vibrational energies are being considered. Photovoltaic devices have not been utilized under indoor, size-constrained conditions until recently since the conventional solar cells utilize bulk materials which are not suitable for small, portable devices. However, third-generation photovoltaic technologies such as organic, dye-sensitized, and perovskite energy sources, have high absorption coefficients and thus low

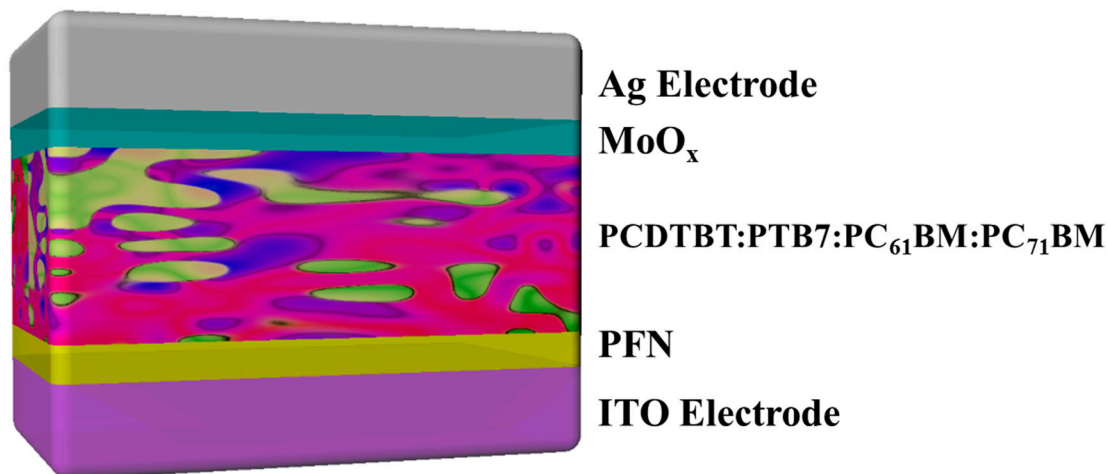
absorber layer thicknesses. They also have the advantage of being flexible and solution-processed, as well as having low manufacturing costs and high absorption in the visible light region [4–6]. These properties make them attractive options for low-power energy harvesting under indoor light sources [7,8]. Organic solar cells have also been extensively researched and, with a tandem structure, have reached nearly 14% efficiency [9], which is higher than the commercialization efficiency of 10%. Steim et al. demonstrated 7% efficiency under fluorescent light using a conventional poly(3-hexylthiophene) (P3HT) and [6,6]-phenyl C₆₁ butyric acid methyl ester (PC₆₁BM) blend [10]. The importance of high shunt resistance and low series resistance in indoor photovoltaics (IPVs) is also discussed. A notable work by Yang et al. and our previous work also discussed the potential of using P3HT:indene-C₆₀ bisadduct (ICBA) as an indoor 500 lx LED light absorber [7,11]. Greater than 20% power conversion efficiency (PCE) has been reported under indoor light illumination [12,13]. Yin et al. reported a ternary photovoltaic cell that could reach a PCE of 20.8%. Cheng et al. demonstrated that ternary bulk heterojunction (BHJ) systems can improve the performance of organic solar cells through improved complimentary absorption of the incoming light, improved charge transport through cascade energy level matching, and improved charge extraction at the BHJ interfaces [14,15]. Their study explained that the use of a cascade energy driver can enhance the driving force for charge transfer [16]. A quaternary solar cell was reported to show good BHJ morphology and charge transport [17]. This article also illustrated that the quaternary solar cell showed improved stability. In spite of these advantages, our optical simulations found that the quaternary photovoltaic was highly sensitive to the active layer thickness. The short-circuit current density (J_{sc}) increased in an oscillatory pattern with respect to the active layer thickness. The quaternary photovoltaic cell exhibited higher oscillations of J_{sc} . The transfer matrix method (TMM) and finite-difference time-domain (FDTD) method are common optical modeling techniques that are used to solve for the distribution of electromagnetic field intensity inside solar cell devices [18–23]. TMM and FDTD can be used to determine the propagation of light using Maxwell's equations. In TMM, each device layer is represented as a matrix and Maxwell's equations are solved as a matrix operation. In FDTD, however, the solar cell device is divided into smaller grids and Maxwell's equations are discretized through approximations and solved for each grid of the device. We utilized a FDTD simulation to determine the number of photons absorbed in the active layer of the quaternary photovoltaic structure under both AM1.5 G and 500 lx white LED illumination. We compared the results with a single BHJ blend of poly({4,8-bis[(2-ethylhexyl)oxy]benzo[1,2-b:4,5-b']dithiophene-2,6-diyl}{3-fluoro-2-[(2-ethylhexyl)carbonyl]thieno[3,4-b]thiophenediyl}) (PTB7) and [6,6]-phenyl C₇₁ butyric acid methyl ester (PC₇₁BM), and another single BHJ blend of Poly[N-9'-hepta-decanyl-2,7-carbazole-alt-5,5-(4',7'-di-2-thienyl-2',1',3'-benzothiadiazole)] (PCDTBT) and PC₇₁BM.

2. Materials and Methods

We performed FDTD simulations using Lumerical FDTD solutions software. The solar cell structures are shown in Figure 1. The complex refractive indices were provided for the individual layer materials of the photovoltaic structures. The thickness of each layer was as follows: Indium tin oxide (ITO) = 150 nm, Poly [(9,9-bis(3'-(N,N-dimethylamino)propyl)-2,7-fluorene)-alt-2,7-(9,9-dioctylfluorene)] (PFN) = 7.7 nm, Molybdenum oxide (MoO_x) = 10 nm, and Ag = 150 nm. The MoO_x acts as a hole transport layer, while the PFN operates as an electron transport layer. A frequency-domain field and power monitor were used to obtain the electric field intensity distribution inside the device structure. A plane wave source was used as the illumination source and was incident at 90°. Periodic boundary conditions were used perpendicular to the source incidence axis and perfectly matched layers were used along the incidence plane. Multi-coefficient fitting of the complex refractive indices and meshing of the device structure were utilized as necessary. The quaternary BHJ ratio was set at 1:9:3:12 of PCDTBT:PTB7:PC₆₁BM:PC₇₁BM, as seen in the reference article by Nam et al. [17]. For the single bulk heterojunction photovoltaic structure we utilized PTB7:PC₇₁BM and PCDTBT:PC₇₁BM-based device structures. The active layer thickness was varied from 50 to 400 nm

and the corresponding electric field intensity inside the active layer was used to measure the number of photons absorbed. By assuming 100% internal quantum efficiency (IQE), the ideal short-circuit current density ($J_{sc,ideal}$) of the photovoltaic cell was obtained. The absorption of the active layer was simulated using the P_{abs} monitor in the software. As this was an optical simulation, the changes to the open circuit voltage (V_{oc}) and fill factor (FF) due to variation in the active layer thickness were assumed to be negligible when compared to the short-circuit current density.

(a)



(b)

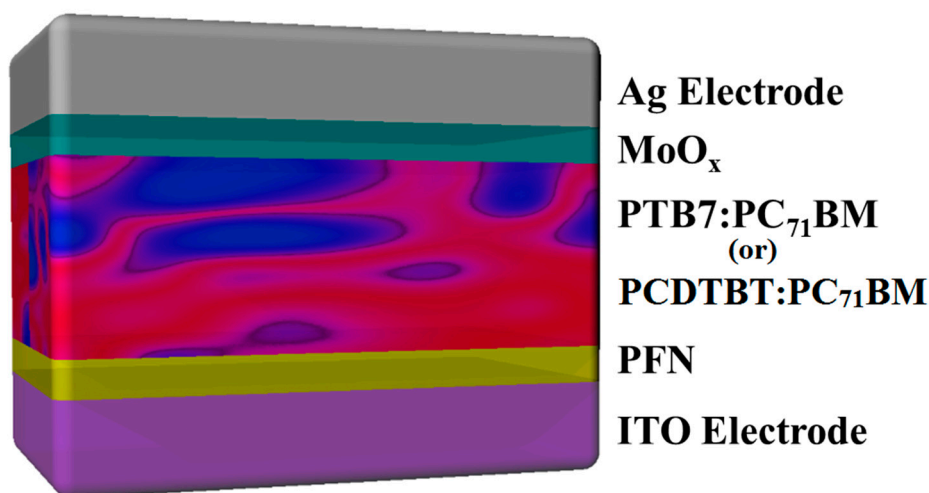


Figure 1. (a) Device structure of the quaternary photovoltaic: ITO/PFN/poly[N-9'-hepta-decanyl-2,7-carbazole-alt-5,5-(4',7'-di-2-thienyl-2',1',3'-benzothiadiazole)];poly[[4,8-bis[(2-ethylhexyl)oxy]benzo[1,2-b:4,5-b']dithiophene-2,6-diyl]][3-fluoro-2-[(2-ethylhexyl)carbonyl]thieno[3,4-b]thiophenediyl]]:[6,6]-phenyl C₆₁ butyric acid methyl ester:[6,6]-phenyl C₇₁ butyric acid methyl ester (PCDTBT:PTB7:PC₆₁BM:PC₇₁BM)/MoO_x/Ag. (b) Device structure of the single bulk heterojunction (BHJ) photovoltaics: ITO/PFN/PTB7:PC₇₁BM/MoO_x/Ag and ITO/PFN/PCDTBT:PC₇₁BM/MoO_x/Ag.

3. Results

FDTD simulations were used to solve approximations of the spatial and temporal derivatives of Maxwell's equations. This can be used to predict the electric and magnetic fields at a discrete future time using knowledge of the fields at a discrete past time. By ensuring that the meshing of the solar cell device structure is small enough to allow for every frequency of the incoming signal to be propagated, the electric field intensity inside the photovoltaic structure could be computed. Since the electric field intensity is directly proportional to the absorbed power, we can calculate the absorption per unit volume as:

$$P_{\text{abs}} = -0.5 \omega |E|^2 \text{imag}(\epsilon) \quad (1)$$

where P_{abs} is the power absorbed per unit volume, $\omega = 2\pi f$ is the angular frequency, E is the electric field intensity, and ϵ is the permittivity.

The number of absorbed photons per unit volume can also be defined in terms of the electric field intensity, as the power absorbed over the energy of a photon:

$$N_{\text{photon}} = (-0.5|E|^2 \text{imag}(\epsilon)) / \hbar \quad (2)$$

where N_{photon} is the number of absorbed photons and \hbar is the reduced Planck constant.

Figure 2a,b compare N_{photon} in the active layers of the quaternary and the single junction photovoltaic cells under LED and AM1.5 G light sources, respectively. N_{photon} is directly proportional to the ideal short-circuit current density ($J_{\text{sc,ideal}}$) that can be obtained from the solar cell's active layer. Thus, $J_{\text{sc,ideal}}$ is the amount of current output that the solar cell will provide per unit area, assuming that the IQE of the solar cell is 100%. It was observed that the quaternary IPV showed higher oscillations in $J_{\text{sc,ideal}}$ with respect to the active layer thickness than the conventional single-junction IPV. This was more evident when the simulation was performed under indoor LED lighting conditions. Due to the elevated oscillatory behavior of $J_{\text{sc,ideal}}$ in the quaternary IPV, it is necessary to carefully choose the proper active layer thickness of the quaternary IPV. By varying the active layer thickness of the quaternary IPV, the electric field intensity produced due to light inside the IPV changes. Through solving for multiple active layer thicknesses in the FDTD simulation, the active layer thickness was optimized to 260 nm under AM1.5 G illumination and 230 nm under 500 lx white LED illumination. It has been shown in previous studies that the optimized active layer thickness varies under different illumination sources [24,25]. Figure 3 shows the optimized quaternary structure obtained by focusing the electric field intensity inside the active layer of the IPV. The absorption window of the quaternary IPV should also overlap with the output of the illumination source for maximum power conversion efficiency. Through our optical simulations, it was found that the absorption of the quaternary and the single junction structure were almost identical when the active layer thickness was set to 230 nm. An active layer thickness of 230 nm was simulated as it represents the thickness at which the maximum number of photons was absorbed in the quaternary IPV (Figure 2a) under indoor light illumination. However, the quaternary photovoltaic showed lower oscillations in absorption with respect to wavelength, as seen in Figure 4a. This leads to a slightly higher overall absorption in the quaternary photovoltaic as compared to the single BHJ counterpart. From Figure S2a,b, it can be observed that the quaternary IPV absorbed more of the incoming radiation than the single BHJ IPV. The quaternary IPV absorbed 79.8% of the LED light spectrum and 65.8% of the AM1.5 G light spectrum. The PTB7:PC₇₁BM-based photovoltaic absorbed 76.4% of the LED light spectrum and 64.8% of the AM1.5 G light spectrum, while the PCDTBT:PC₇₁BM-based photovoltaic absorbed 72.5% of the LED light spectrum and 52.7% of the AM1.5 G light spectrum. This shows that the absorption profile of the quaternary IPV is slightly better than a more conventional, high-efficiency, single-junction solar cell structure such as PTB7:PC₇₁BM. Therefore, there is high potential for the quaternary heterojunction to be used as an active layer mixture for IPV, as its absorption is independent of oscillations for a wide wavelength range. Comparably, the quaternary mixture is superior to the

single BHJ in both its absorption curve and the tendency of N_{photon} to increase steadily with respect to the active layer thickness.

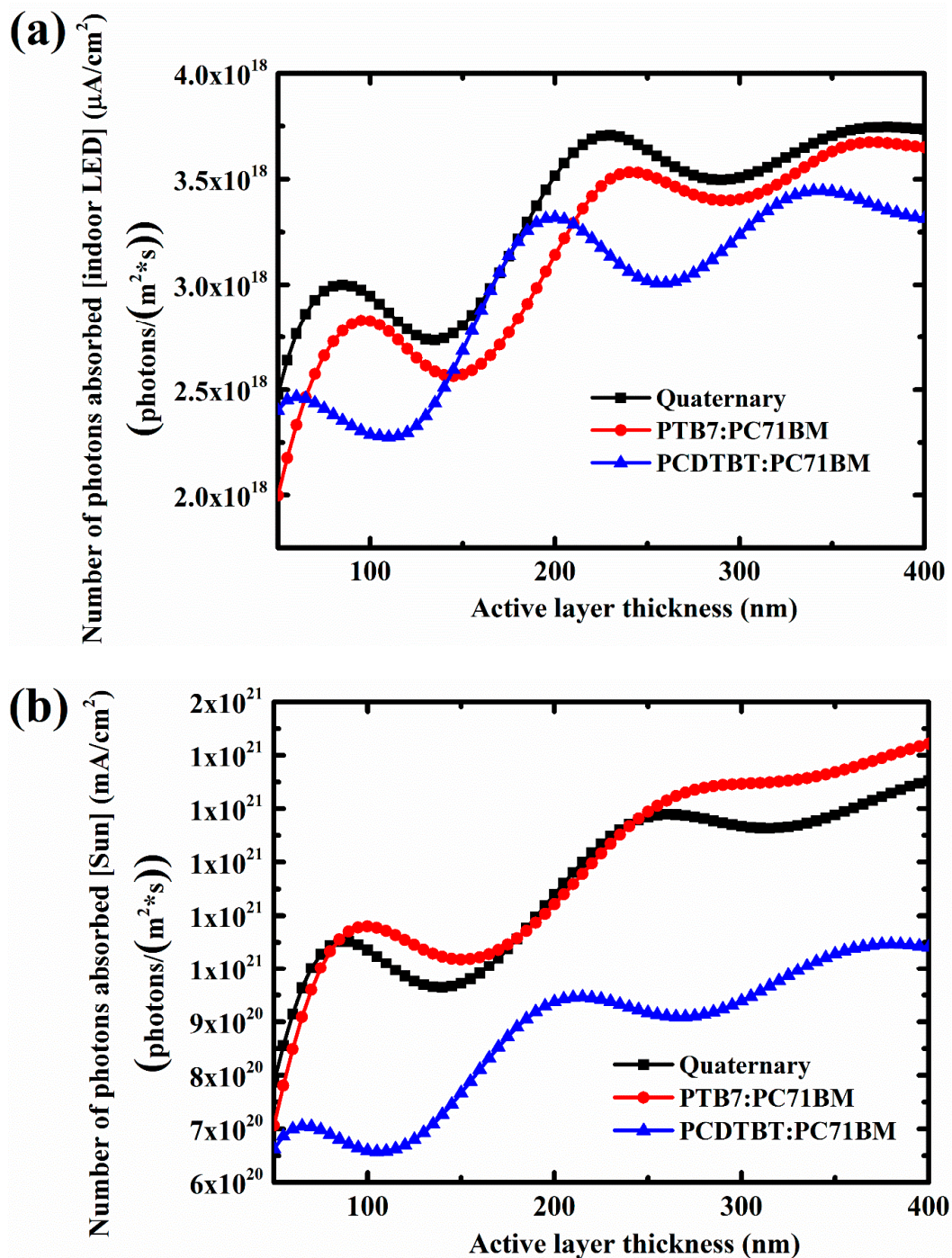


Figure 2. Assuming 100% IQE, the ideal short-circuit current density ($J_{\text{sc,ideal}}$) was simulated. (a) The number of photons absorbed (which directly relates to the $J_{\text{sc,ideal}}$) in quaternary and single BHJ photovoltaic cells under indoor LED illumination. (b) The number of photons absorbed in quaternary and single BHJ photovoltaic cells under AM1.5 G illumination.

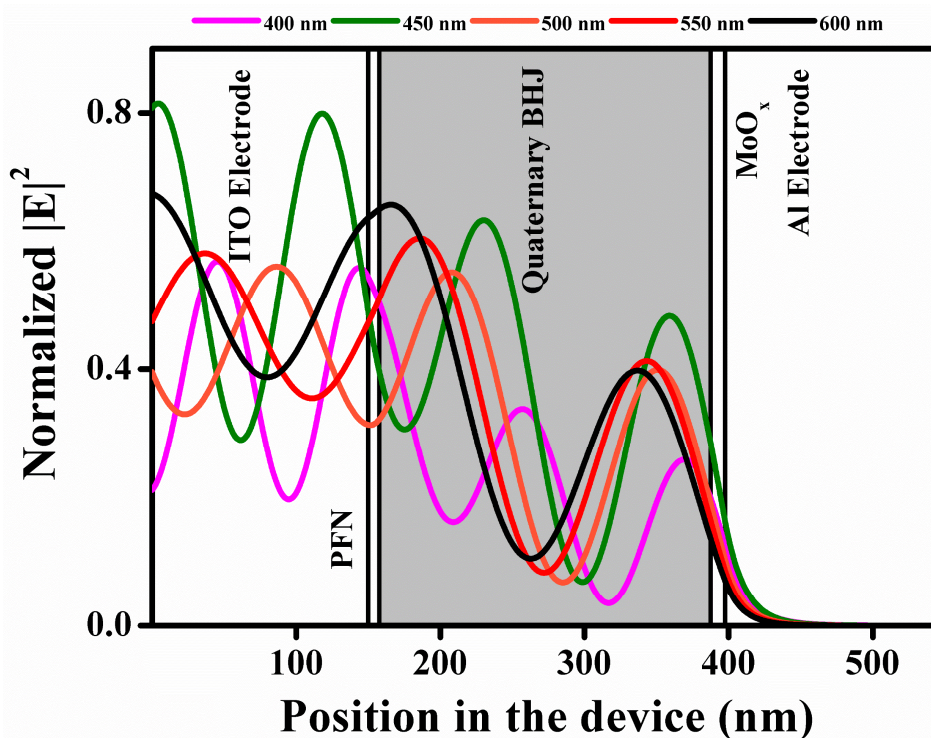


Figure 3. Electric field intensity distribution inside the photovoltaic structure obtained through a finite-difference time-domain (FDTD) simulation. The thickness of the active layer was 230 nm, which showed peak absorption under 500 lx indoor white LED illumination.

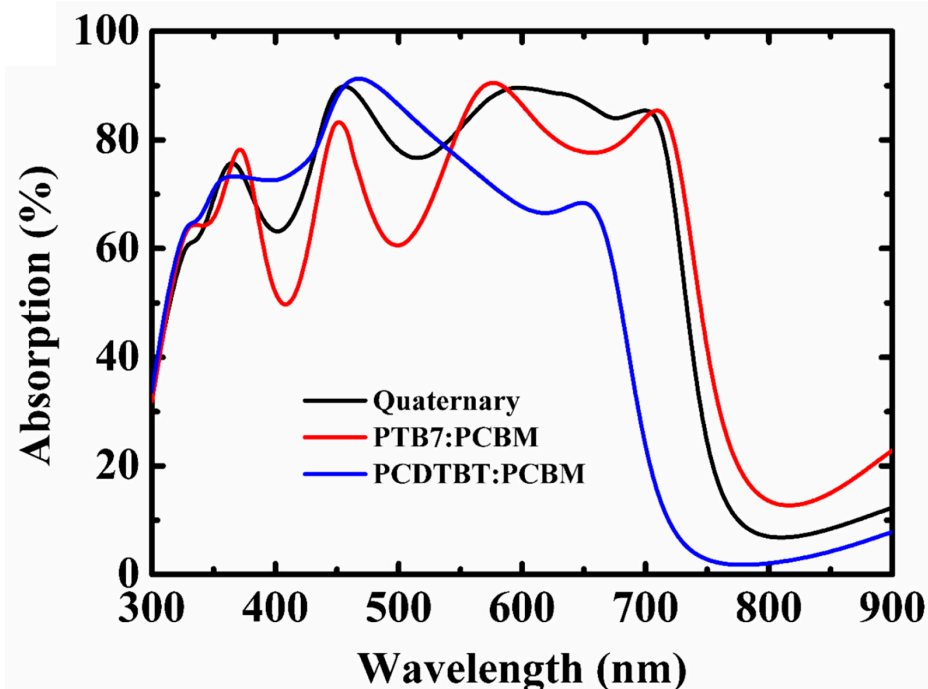


Figure 4. The absorption of quaternary and single BHJ active layers at a thickness of 230 nm. The single BHJs showed absorption similar to the quaternary indoor photovoltaic (IPV), with the quaternary IPV exhibiting a slightly higher absorption than PTB7:PC₇₁BM, and a slightly lower absorption than PCDTBT:PC₇₁BM at ~450 nm wavelength (LED spectrum's peak).

4. Discussion

Nam et al. published results in which quaternary solar cells showed better charge transport and morphological structuring than their single junction counterparts [17]. Since we observed that the optical absorption is almost similar to single junction photovoltaic cells, we hypothesized that the better efficiency of the quaternary solar cells discussed in the study was largely due to the better charge transport and extraction properties of the quaternary layer, thus strengthening the claim of the article. PTB7 has an absorption peak at ~600 to 700 nm, which lies outside of the input light spectrum. Thus, in the quaternary IPV the PCDTBT donor polymer would dominate the light absorption, as its absorption peak is at ~400 to 550 nm, which is complementary to that of PTB7. Thus, PTB7 aids in charge transport by acting as a cascade energy level. By improving the hole charge mobility and lowering the recombination rate, the PTB7 donor in the quaternary blend acts primarily as a charge transport enhancer and secondarily as a complimentary incoming light absorber [13,26,27]. Although the peak absorption of PTB7 is outside of the spectral range of the incoming light, we hypothesized that it might contribute to some of the absorbed light based on the results presented in Figures 2 and 4. The quaternary IPV has prominent peaks in the $J_{sc,ideal}$ curve and lower oscillations in the absorption curve. The oscillatory pattern of the $J_{sc,ideal}$ curve of the quaternary IPV (Figure 2a) are similar to those of the PTB7 BHJ IPV, while the peaks of the oscillatory curve of the quaternary IPV in Figure 2a are between those of the PTB7 and PCDTBT BHJ IPV. We investigated the reason behind this oscillatory behavior in Figure S1a–e, which show the electric field intensity distribution inside the photovoltaic devices. When the light traverses through the photovoltaic device it reflects, diffracts, and transmits through the different layers due to the variations in the refractive indices of the layers. Moreover, the Ag electrode reflects all the light back into the device, thus acting as a mirror. Due to these effects, the incoming and the reflected light waves interact constructively and destructively. These interactions caused hot spots and cold spots inside of the device, where the photons are concentrated or depleted. Finite-difference time-domain simulations were used to simulate these hot spots inside of the device for active layer thicknesses of 100, 150, 200, 250, and 300 nm (Figure S1). The LED spectrum, which is provided in Figure S2a, was observed to have maxima peaks at ~450 and ~550–600 nm. In Figure S1a the hot spot was around ~450 nm, which was a maximum in the LED spectrum. Moreover, wavelengths from 400 to 600 nm were concentrated inside the 100 nm thick active layer of the photovoltaic device. In Figure S1b, where the active layer thickness was 150 nm, the hot spot moved to approximately the 500 to 550 nm wavelength range. The LED spectrum was not concentrated in this wavelength range, resulting in a dip in the $J_{sc,ideal}$ curve in Figure S2a. Figure S1c,d show considerable absorption in the wavelength regions of 450 to 600 nm. Although they both possessed a cold spot cutting through the active layer, the higher thickness of the active layer helped them to absorb more incoming photons than the previous device structures. Finally, Figure S1e shows very little electric field intensity concentrated inside the active layer (highest at ~525 nm). This consequently led to the second drop in the oscillating $J_{sc,ideal}$ curve after it reached its maximum at an active layer thickness of ~230 nm. Thus, it can be concluded that the oscillatory nature seen in Figure 2a was due to the interference of the incident and reflected light traversing through the different refractive index layers of the device. We also believe that the complimentary absorption of both PCDTBT and PTB7 contribute to the lower oscillations in the absorption seen in Figure 4. We hypothesized that PTB7 had absorbed a small part of the incoming light, which contributed to the unique characteristics of the quaternary IPV, while PCDTBT was the main light absorber. Thus, the quaternary IPV exhibited hybrid characteristics obtained from both PTB7 and PCDTBT components. We discussed the viability of the quaternary IPV for indoor light harvesting applications in our previous article [24]. This article mentioned that the IPV was observed to have low series resistance and high shunt resistance, even under low light conditions. This proved that the V_{oc} and FF of the IPV were satisfactorily high, similar to those of the photovoltaics illuminated under an AM1.5 G source. The current study further observed that $J_{sc,ideal}$ is highly dependent on the active layer thickness when illuminated under an LED light source.

5. Conclusions

We utilized FDTD simulations to solve for the electric field intensity inside a quaternary photovoltaic structure. We found that the absorption of the quaternary IPV was highly dependent on the active layer thickness when illuminated under LED light due to the high oscillations in $J_{sc,ideal}$. We found that the maximum $J_{sc,ideal}$ was observed at an active layer thickness of 260 nm under AM1.5 G illumination and at a thickness of 230 nm under 500 lx indoor LED illumination. The absorption of the quaternary photovoltaic cells was found to be uncompromised and exhibited similar, yet slightly higher, absorption to conventional, high-efficiency PTB7:PC₇₁BM and PCDTBT:PC₇₁BM-based photovoltaic cell. We also observed that the quaternary IPV obtained certain light absorption characteristics from its individual donors. We believe this leads to both cascade charge transfer and parallel-like charge transfer between the donors and acceptors, with PTB7 acting primarily as a cascade energy level for better hole extraction to the cathode.

Supplementary Materials: The following are available online at <http://www.mdpi.com/1996-1073/12/10/1838/s1>, Figure S1: Electric field intensity distribution in the quaternary photovoltaic: ITO/PFN/PCDTBT:PTB7:PC61BM:PC71BM/MoO_x/Ag. (a) Active layer thickness = 100 nm. (b) Active layer thickness = 150 nm. (c) Active layer thickness = 200 nm. (d) Active layer thickness = 250 nm. (e) Active layer thickness = 300 nm. Figure S2: (a) Amount of 500 lx white LED spectrum absorbed by both quaternary and single BHJ photovoltaics. (b) Amount of AM1.5 G spectrum absorbed by both quaternary and single BHJ photovoltaics.

Author Contributions: Conceptualization, J.W.S., J.-H.B., and H.K.; Data curation, P.V.; Formal analysis, P.V., J.J., I.M.K., P.L., J.-H.B., and H.K.; Funding acquisition, J.W.S., J.-H.B., and H.K.; Investigation, P.V.; Methodology, P.V. and H.K.; Project administration, J.-H.B. and H.K.; Resources, J.W.S.; Software, P.V. and J.W.S.; Supervision, J.-H.B.; Validation, J.J., I.M.K., P.L., J.-H.B., and H.K.; Visualization, P.V.; Writing—original draft, P.V.; Writing—review and editing, P.V., J.-H.B., and H.K.

Funding: This research received no external funding.

Acknowledgments: This research was supported by the Basic Science Research Program through the National Research Foundation of Korea (NRF) funded by the Ministry of Science and ICT (2018R1A2B6008815 and 2018R1D1A3B07049992), and also by the BK21 Plus project funded by the Ministry of Education, Korea (21A20131600011). H.K. also would like to acknowledge the funding by MOTIE (Ministry of Trade, Industry and Energy) (project number 10063473). This work was also supported by the Korea institute of Energy Technology Evaluation and Planning (KETEP) and the Ministry Of Trade, Industry and Energy (MOTIE) of the Republic of Korea (no. 20194030202320).

Conflicts of Interest: The authors declare no conflict of interest. The funders had no role in the design of the study; in the collection, analyses, or interpretation of data; in the writing of the manuscript, or in the decision to publish the results.

References

- Sharma, H.; Haque, A.; Jaffery, Z.A. Solar energy harvesting wireless sensor network nodes: A survey. *J. Renew. Sustain. Energy* **2018**, *10*, 23704. [[CrossRef](#)]
- Varghese, B.; John, N.E.; Sreelal, S.; Gopal, K. Design and development of an RF energy harvesting wireless sensor node (EH-WSN) for aerospace applications. *Procedia Comput. Sci.* **2016**, *93*, 230–237. [[CrossRef](#)]
- Rashidzadeh, H.; Kasargod, P.S.; Supon, T.M.; Rashidzadeh, R.; Ahmadi, M. Energy harvesting for IoT sensors utilizing MEMS technology. In Proceedings of the 2016 IEEE Canadian Conference on Electrical and Computer Engineering (CCECE), Vancouver, BC, Canada, 5–18 May 2016; pp. 1–4.
- Lu, L.; Zheng, T.; Wu, Q.; Schneider, A.M.; Zhao, D.; Yu, L. Recent advances in bulk heterojunction polymer solar cells. *Chem. Rev.* **2015**, *115*, 12666–12731. [[CrossRef](#)] [[PubMed](#)]
- Chiechi, R.C.; Havenith, R.W.A.; Hummelen, J.C.; Koster, L.J.A.; Loi, M.A. Modern plastic solar cells: Materials, mechanisms and modeling. *Mater. Today* **2013**, *16*, 281–289. [[CrossRef](#)]
- Chamberlain, G.A. Organic solar cells: A review. *Sol. Cells* **1983**, *8*, 47–83. [[CrossRef](#)]
- Vincent, P.; Shin, S.-C.; Goo, J.S.; You, Y.-J.; Cho, B.; Lee, S.; Lee, D.-W.; Kwon, S.R.; Chung, K.-B.; Lee, J.-J.; et al. Indoor-type photovoltaics with organic solar cells through optimal design. *Dye. Pigment.* **2018**, *159*, 306–313. [[CrossRef](#)]
- Shin, S.-C.; Koh, C.W.; Vincent, P.; Goo, J.S.; Bae, J.-H.; Lee, J.-J.; Shin, C.; Kim, H.; Woo, H.Y.; Shim, J.W. Ultra-thick semi-crystalline photoactive donor polymer for efficient indoor organic photovoltaics. *Nano Energy* **2019**, *58*, 466–475. [[CrossRef](#)]

9. Cheng, P.; Li, G.; Zhan, X.; Yang, Y. Next-generation organic photovoltaics based on non-fullerene acceptors. *Nat. Photonics* **2018**, *12*, 131–142. [[CrossRef](#)]
10. Steim, R.; Ameri, T.; Schilinsky, P.; Waldauf, C.; Dennler, G.; Scharber, M.; Brabec, C.J. Organic photovoltaics for low light applications. *Sol. Energy Mater. Sol. Cells* **2011**, *95*, 3256–3261. [[CrossRef](#)]
11. Yang, S.-S.; Hsieh, Z.-C.; Keshtov, M.L.; Sharma, G.D.; Chen, F.-C. Toward high-performance polymer photovoltaic devices for low-power indoor applications. *Sol. RRL* **2017**, *1*, 1700174. [[CrossRef](#)]
12. Cutting, C.L.; Bag, M.; Venkataraman, D. Indoor light recycling: A new home for organic photovoltaics. *J. Mater. Chem. C* **2016**, *4*, 10367–10370. [[CrossRef](#)]
13. Yin, H.; Ho, J.K.W.; Cheung, S.H.; Yan, R.J.; Chiu, K.L.; Hao, X.; So, S.K. Designing a ternary photovoltaic cell for indoor light harvesting with a power conversion efficiency exceeding 20%. *J. Mater. Chem. A* **2018**, *6*, 8579–8585. [[CrossRef](#)]
14. Cheng, P.; Wang, J.; Zhang, Q.; Huang, W.; Zhu, J.; Wang, R.; Chang, S.-Y.; Sun, P.; Meng, L.; Zhao, H.; et al. Unique energy alignments of a ternary material system toward high-performance organic photovoltaics. *Adv. Mater.* **2018**, *30*, 1801501. [[CrossRef](#)] [[PubMed](#)]
15. Cheng, P.; Wang, R.; Zhu, J.; Huang, W.; Chang, S.-Y.; Meng, L.; Sun, P.; Cheng, H.-W.; Qin, M.; Zhu, C.; et al. Ternary system with controlled structure: A New strategy toward efficient organic photovoltaics. *Adv. Mater.* **2018**, *30*, 1705243. [[CrossRef](#)]
16. Cheng, P.; Zhang, M.; Lau, T.-K.; Wu, Y.; Jia, B.; Wang, J.; Yan, C.; Qin, M.; Lu, X.; Zhan, X. Realizing small energy loss of 0.55 eV, high open-circuit voltage >1 v and high efficiency >10% in fullerene-free polymer solar cells via energy driver. *Adv. Mater.* **2017**, *29*, 1605216. [[CrossRef](#)] [[PubMed](#)]
17. Nam, M.; Cha, M.; Lee, H.H.; Hur, K.; Lee, K.-T.; Yoo, J.; Han, I.K.; Kwon, S.J.; Ko, D.-H. Long-term efficient organic photovoltaics based on quaternary bulk heterojunctions. *Nat. Commun.* **2017**, *8*, 14068. [[CrossRef](#)] [[PubMed](#)]
18. Monestier, F.; Pandey, A.K.; Simon, J.-J.; Torchio, P.; Escoubas, L.; Nunzi, J.-M. Optical modeling of the ultimate efficiency of pentacene: N, N'-ditridecylperylene-3, 4, 9, 10-tetracarboxylic diimide–blend solar cells. *J. Appl. Phys.* **2007**, *102*, 34512. [[CrossRef](#)]
19. Monestier, F.; Simon, J.-J.; Torchio, P.; Escoubas, L.; Ratier, B.; Hojeij, W.; Lucas, B.; Moliton, A.; Cathelinaud, M.; Defranoux, C.; et al. Optical modeling of organic solar cells based on CuPc and C60. *Appl. Opt.* **2008**, *47*, C251–C256. [[CrossRef](#)]
20. Duche, D.; Torchio, P.; Escoubas, L.; Monestier, F.; Simon, J.-J.; Flory, F.; Mathian, G. Improving light absorption in organic solar cells by plasmonic contribution. *Sol. Energy Mater. Sol. Cells* **2009**, *93*, 1377–1382. [[CrossRef](#)]
21. Vincent, P.; Bae, J.-H.; Kim, H. Efficiently-designed hybrid tandem photovoltaic with organic and inorganic single cells. *J. Korean Phys. Soc.* **2016**, *68*, 1094–1098. [[CrossRef](#)]
22. Vincent, P.; Song, D.-S.; Kwon, H.B.; Kim, D.-K.; Jung, J.-H.; Kwon, J.-H.; Choe, E.; Kim, Y.-R.; Kim, H.; Bae, J.-H. Towards maximizing the haze effect of electrodes for high efficiency hybrid tandem solar cell. *Appl. Surf. Sci.* **2018**, *432*, 262–265. [[CrossRef](#)]
23. Vincent, P.; Song, D.-S.; Jung, J.-H.; Kwon, J.-H.; Kwon, H.B.; Kim, D.-K.; Choe, E.; Kim, Y.-R.; Kim, H.; Bae, J.-H. Dependence of the hybrid solar cell efficiency on the thickness of ZnO nanoparticle optical spacer interlayer. *Mol. Cryst. Liq. Cryst.* **2017**, *653*, 254–259. [[CrossRef](#)]
24. Shin, S.-C.; Vincent, P.; Bae, J.-H.; Lee, J.J.; Nam, M.; Ko, D.-H.; Kim, H.; Shim, J.W. Quaternary indoor organic photovoltaic device demonstrating panchromatic absorption and power conversion efficiency of 10%. *Dye. Pigment.* **2019**, *163*, 48–54. [[CrossRef](#)]
25. Vincent, P.; Shim, J.W.; Bae, J.-H.; Kim, H. Optimizing the efficiency of organic solar cell under indoor light via controlling optical absorption. *Mol. Cryst. Liq. Cryst.* **2018**, *660*, 85–89. [[CrossRef](#)]
26. Khlyabich, P.P.; Burkhart, B.; Thompson, B.C. Efficient ternary blend bulk heterojunction solar cells with tunable open-circuit voltage. *J. Am. Chem. Soc.* **2011**, *133*, 14534–14537. [[CrossRef](#)]
27. Heidel, T.D.; Hochbaum, D.; Sussman, J.M.; Singh, V.; Bahlke, M.E.; Hiromi, I.; Lee, J.; Baldo, M.A. Reducing recombination losses in planar organic photovoltaic cells using multiple step charge separation. *J. Appl. Phys.* **2011**, *109*, 104502. [[CrossRef](#)]

